The International Journal of Advanced Manufacturing Technology (2019) 103:3151–3161
https://doi.org/10.1007/s00170-019-03761-8

ORIGINAL ARTICLE

Finite element simulation analysis of bionic ball-end milling cutter

Wei Zhang [1,2] · Lei Zhang [1] · Ben Wang [1] · Shuqi Wang [1]

Received: 31 October 2018 / Accepted: 15 April 2019 / Published online: 8 May 2019

Abstract

In the process of cutting titanium alloy by ball-end milling cutter, the surface quality of the workpiece is difficult to guarantee, and the cutting force is the main factor affecting the surface quality of the workpiece. Aiming at the above problems, the bionic structure is combined with the ball-end milling cutter to simulate the bionic ball-end milling cutter. Firstly, the forming process of the machined surface during the cutting process of the ball-end milling cutter is analyzed, and the effective cutting speed of the ball-end milling cutter is solved, the geometric model of equivalent cutting thickness is established. Finally, the finite element model of the bionic ball-end milling cutter was established to study the equivalent stress state of the workpiece under different bionic structure types, and the influence of bionic structure on the cutting force was analyzed. The conclusions obtained provide a theoretical basis for the selection of parameters for the preparation of bionic ball-end milling cutters.

Keywords Ball-end mill · Titanium alloy · Bionic · Stress · Cutting force

1 Introduction

Titanium alloy is widely used in the aerospace industry due to its excellent specific strength and good corrosion resistance, and has quickly become one of the main structural materials in this field. The proportion of titanium alloy on the body of advanced aerospace engines is increasing rapidly. Titanium alloy has become one of the indispensable materials for the development of aerospace industry. However, the process performance of titanium alloy is poor, and the cutting process is difficult, which affects the dimensional accuracy of the machined surface, and has become a problem in the aerospace manufacturing industry.

The surface quality of the workpiece during the cutting of titanium alloy is difficult to guarantee, and the cutting force is the main cause of this phenomenon. The existing researches show that the surface of various bionic structures has good mechanical properties. In order to reduce the cutting force in the process of cutting titanium alloy, the bionic structure and the ball-end milling cutter are combined to study the cutting performance of the micro-textured ball-end milling cutter. Etsion [1, 2] studies have shown that a suitable laser surface micro-texture can improve the friction characteristics of the mechanical parts surface and improve the load-carrying capacity. Zheng [3] used laser to process the bionic micro-textured surface and studied the wear performance in parallel, and the results show that the micro-textured surface has better wear resistance. Thepsonthi [4] studied the role of coated tools in the micromachining of Ti-6Al-4V titanium alloy and revealed the effect of micro-end milling cutter on cutting force generation, tool temperature, contact pressure, and sliding speed. Kawasegi [5] machined the micron and nano groove texture on the rake face of the turning tool. The cutting force of the micro-texture is lower when the cutting speed reaches 420 m/min, and the friction of the rake face is caused by the insertion of the texture. Lowering the groove texture perpendicular to the chip outflow direction has a better antifriction effect. Zhang [6] prepared the texture morphology on the surface of TiAlN coated tool, carried out the AISI1045 hardened steel cutting experiment under the condition of trace and full lubrication, and analyzed the cutting performance of the tool. The results show that the cutting performance of the texture tool is better. Ronen [7] processed the surface of pits with different sizes on the piston ring. The friction and wear experiments showed that the average friction of the piston ring specimen with the concave surface was 30% smaller than that

✉ Lei Zhang
2305647762@qq.com

[1] College of Mechanical and Power Engineering, Harbin University of Science and Technology, Harbin 150080, China

[2] Measurement-control Technology and Instrument Key Laboratory of Universities in Heilongjiang province, Harbin University of Science and Technology, Harbin 150080, China

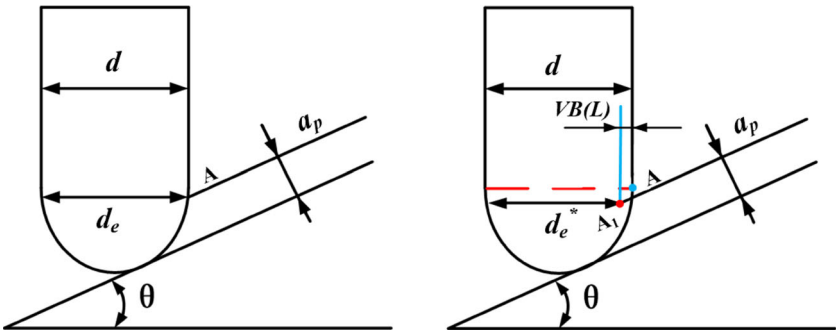

(a) Tool is not worn (b)Tool wear

Fig. 1 Ball-end milling cutter cutting bevel. (**a**) Tool is not worn. (**b**) Tool wear

of the ordinary test piece. Enomoto [8] processed a groove-like micro-texture of a certain density at the rake face of the insert near the cutting edge. It was found through experiments that the micro-texture can improve the anti-bonding of the tool during dry cutting and wet cutting.

Lei [9] used finite element software to analyze the influence of micro-pits on the rake face on the mechanical properties of the tool and then used the femtosecond laser processing technology to prepare the cemented carbide tool with micro-pits, and it was found that the average cutting force of the tool with micro-pits on the rake face was reduced by 10–30% compared to the conventional tool. Rao [10] analyzed the cutting geometry model of contour surface milling and calculated the chip thickness variation during machining by continuously simulating the tool path. Mhamdi [11] analyzed the inclination angle of the cutting path of the tool and obtained the influence of the milling cutter position and cutting process parameters on the surface morphology of the machining process when the ball-end milling cutter was used to process the free-form surface mold. Senatore [12] studied the problem of tool structure selection and milling spacing in surface machining. Jiang [13] designed the cutting edge of the milling cutter by observing the appearance and structure of the corn leaf. The experiment and simulation were compared with the ordinary milling cutter. The experimental results show that the biomimetic structure can effectively suppress the tool vibration. Zhong [14] studied the surface of bionic non-smooth organisms and found that the non-smooth surface has the characteristics of reducing resistance, anti-sticking, and anti-friction. The bionic non-smooth theory is applied to the design of diamond drill bits, and it has been found through experiments that it has great advantages compared with conventional drill bits. Sczerzenie [15] considered the size effect of the tool and the anisotropy of the structure, the surface integrity and chip formation process in the ultra-precision cutting titanium alloy orthogonal test were studied, and the surface morphology and the formation of the burr were studied in detail. Yao [16] analyzed the effects of processing parameters on three-dimensional surface topography and fatigue life through high-speed milling and fatigue life test, and the fracture mechanism of fatigue specimens was used to reveal the mechanism of surface morphology on fatigue cracks. Honghua [17] used PCD and carbide tools for high-speed finishing TA15 wear test and studied the service life of PCD and carbide tools. Razfar [18] proposed that the surface topography of the workpiece has a great influence on the performance of the workpiece, such as fatigue resistance, surface friction, wear, light reflection, and heat transfer. Ren [19] has carried out biomimetic studies on the surface of a large number of crustaceans and found that there are many pits and groove structures in the living body table, and applying the bionic structure to agricultural equipment can reduce the adhesion of mechanical surfaces and soil. It has an important influence on the size and arrangement of the microstructure of the organism. Peng [20] studied the formation of surface topography, surface texture interval, surface texture height, and surface texture direction by simulation and experiment, and proposed a method to control the surface texture direction.

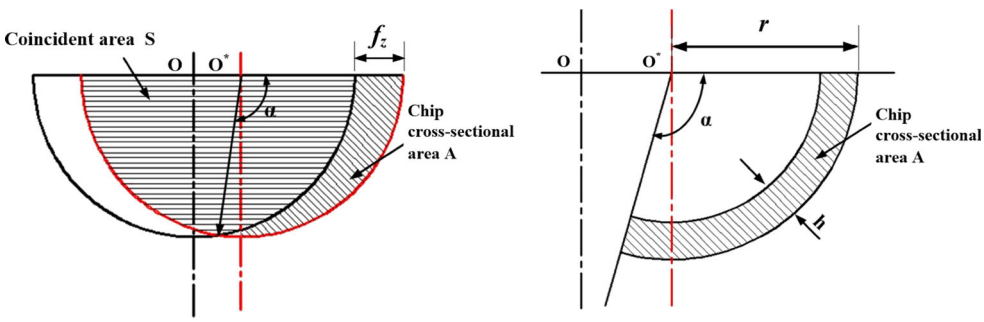

(a) Chip cross-sectional area (b) Equivalent cross-sectional area

Fig. 2 Chip formation process. (**a**) Chip cross-sectional area. (**b**) Equivalent cross-sectional area

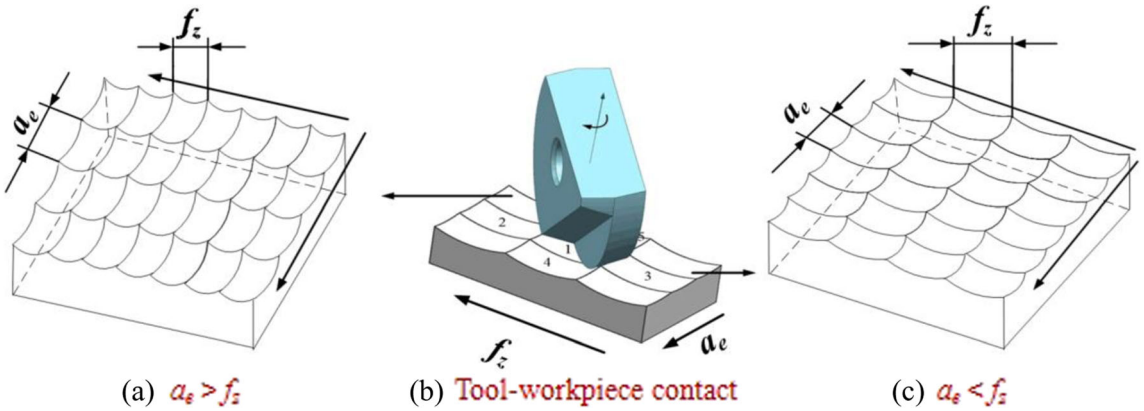

Fig. 3 Machined surface topography by ball-end cutter

In order to further reduce the cutting force generated by the ball-end milling cutter during the process of cutting titanium alloy, on the basis of establishing the idea and application of bionic design, the bionic structure and the ball-end milling cutter are combined to prepare the micro-textured ball-end milling cutter. A finite element analysis model was established to analyze the distribution of equivalent stress states on the workpiece surface by different texture types.

2 Ball-end milling cutter milling surface forming principle

2.1 Effective cutting speed of ball-end mill

The ball-end milling cutter has an effective cutting radius of 0 at the tool tip during the cutting process, so the cutting speed at the tool tip is also zero. The tip of the tool participates in the cutting, which leads to the degradation of the surface quality of the workpiece and reduces the service life of the tool. During the cutting process, the cutting speed of the cutting edge varies with the position of the contact point of the tool and the workpiece. The cutting condition in which the cutting workpiece is inclined at an angle θ when the ball-end mill is not worn is as shown in Fig. 1(a).

d is the tool diameter, d_e is the effective cutting diameter, a_p is the cutting depth, and θ is the workpiece inclination angle. d_e^* is the effective cutting diameter after the tool wears, and VB is the effective cutting diameter difference before and after the tool wear.

$$d_e = d\sin\left(\theta + \cos^{-1}\frac{d-2a_p}{d}\right) \tag{1}$$

$$v_{min} = \pi\, d\, n\sin\theta \tag{2}$$

$$v_{max} = \pi\, d\, n\sin\left(\theta + \cos^{-1}\frac{d-2a_p}{d}\right) \tag{3}$$

When the ball-end mill wears, the highest cutting point on the cutting edge moves from A to A_1. After wear, the effective diameter of the ball-end mill is:

Table 1 Different bionic structure morphology of the cutting edge

No texture	Pit texture	Vertical groove	Transverse groove	Orthogonal micro-texture	Offset angle 0.3°
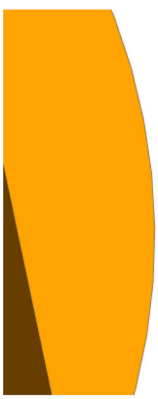	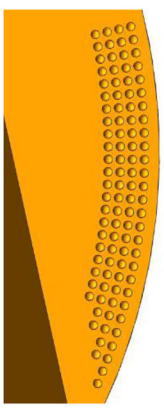	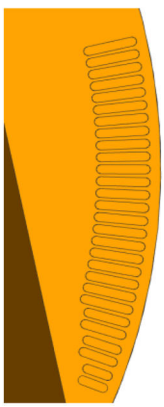	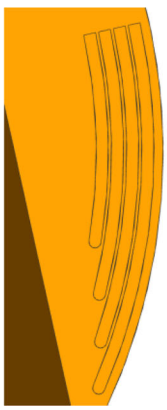	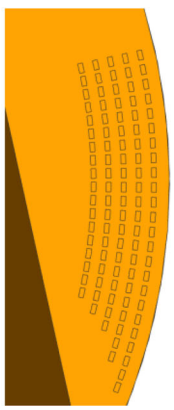	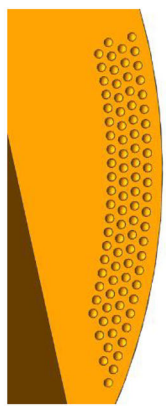

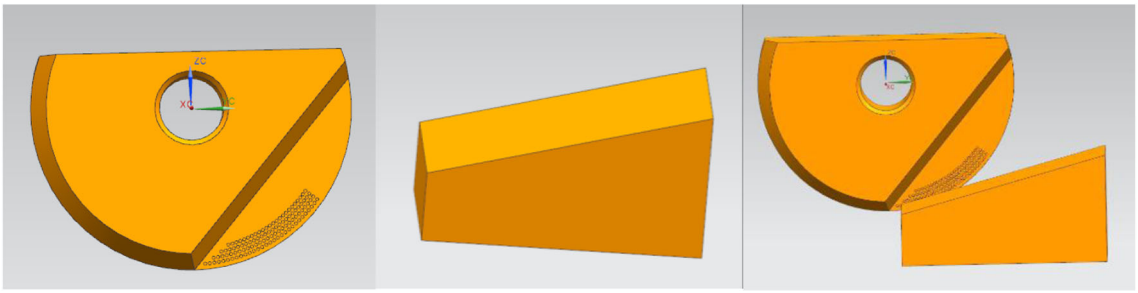

Fig. 4 The relationship between tool and workpiece assembly

$$d_e{}^{*} = (d-\mathrm{VB})\sin\left(\theta + \cos^{-1}\frac{d-2a_p}{d}\right) \tag{4}$$

It can be seen that as the amount of wear on the rake face increases, the maximum effective cutting diameter decreases, resulting in a decrease in the actual maximum effective cutting speed. The cutting speed in turn causes a change in the cutting environment, and the cutting force, cutting temperature, and tool life will both have an impact.

2.2 Calculation of equivalent cutting thickness

The shape of the chip cross section is the portion surrounded by the trajectories of the adjacent two teeth, so the chip thickness is continuously changed. The feed per tooth and the tool radius determine the geometry of the chip. The chip formation process is shown in Fig. 2.

α is the chip angle, f_z is the feed per foot, r is the cutting radius, h is the equivalent cutting thickness, A is the chip cross-sectional area, S is the coincident portion of two consecutive cuts, and the chip angle α shown in Fig. 2(a) is:

$$\alpha = \pi - \cos^{-1}\frac{f_z}{2r} \tag{5}$$

The cross-sectional area A of the chip is:

$$A = \frac{1}{2}\pi r^2 - S \tag{6}$$

The coincident portion S of two consecutive cuts is:

$$S = \frac{1}{2}r^2\left[2\cos^{-1}\frac{f_z}{2r} - \sin\left(2\cos^{-1}\frac{f_z}{2r}\right)\right] \tag{7}$$

Bring Eq. (7) into Eq. (6) is:

$$A = \frac{1}{2}r^2\left[\pi - 2\cos^{-1}\frac{f_z}{2r} - \sin\left(2\cos^{-1}\frac{f_z}{2r}\right)\right] \tag{8}$$

The chip thickness is continuously variable, and since the feed per tooth is small and the rotational speed of the tool is high, so the thickness change is small. The continuously changing chips are simplified into equivalent chips of uniform thickness distribution, and the equivalent cutting thickness shown in Fig. 2(b) is:

$$h = r - \sqrt{r^2 - 2\frac{A}{\alpha}} = r - r\sqrt{\frac{\cos^{-1}\frac{f_z}{2r} - \sin\left(2\cos^{-1}\frac{f_z}{2r}\right)}{\pi - 2\cos^{-1}\frac{f_z}{2r}}} \tag{9}$$

2.3 Machined surface formation process

Due to the influence of the tool itself and the trajectory of the tool, there are residual tool marks on the surface of the workpiece, and these tool marks constitute the processed surface topography. The ball-end mill rotates 1 week to form a sphere, and the surface of the workpiece can be simplified into a sphere to perform Boolean operations on the workpiece. The surface of the ball-end mill after cutting the workpiece is composed of a plurality of small pits surrounded by four ridge lines, as shown in Fig. 3.

Figure 3 shows the contact relationship of the tool-workpiece. Since the line spacing a_e is large and the feed per foot f_z is small, the surface topography formed by the ball-end mill

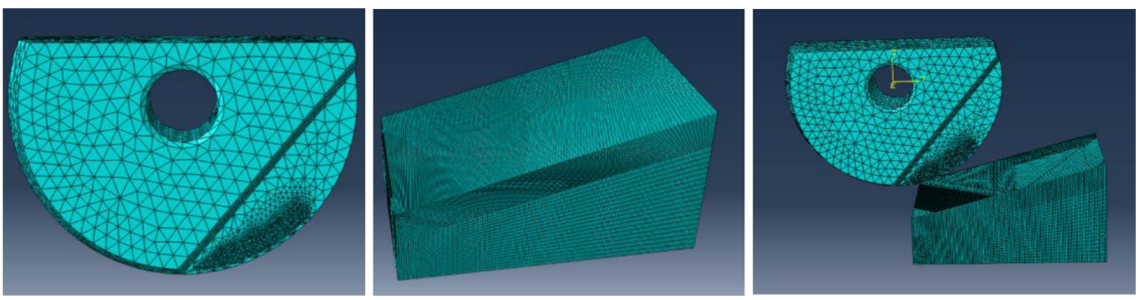

Fig. 5 Finite element model meshing

Table 2 Meshing of cutting edges of different bionic structure

No texture	Pit texture	Vertical groove	Transverse groove	Orthogonal micro-texture	Offset angle 0.3°
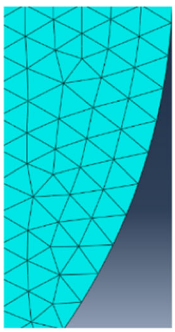	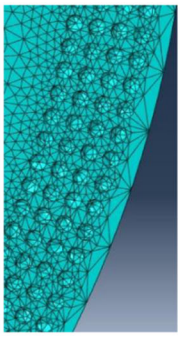	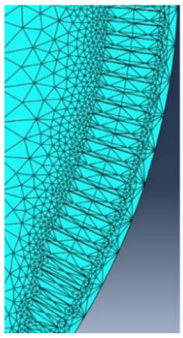	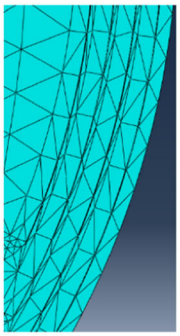	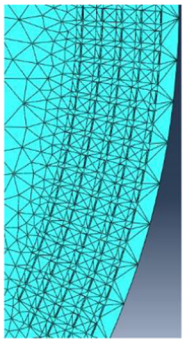	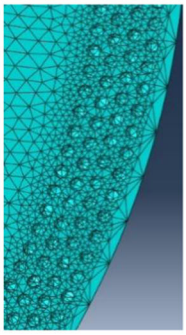

cutting is shown in Fig. 3a. Since the feed per foot f_z is large and the line spacing a_e is very small, the surface topography formed by the ball-end mill cutting is shown in Fig. 3(c).

3 Geometric model building and meshing

3.1 Establishment of geometric models

The first step in the establishment of the finite element model is to transform the entity into a geometric model that accurately describes the spatial geometric relationship of the entity and facilitates the division of elements and nodes. Three-dimensional modeling in UG software, the overall size of the geometric model, is not conducive to the calculation of the solution, the corresponding simplified processing of the tool only modeling the blade part.

The rake face of the tool is placed into the pit texture, the vertical groove, the transverse groove, and the orthogonal micro-texture. At the same time, the texture of the different lengths and different offset angles of the cutting edge is designed for the pit texture. Considering the influence of the bionic structure on the tool strength and the size of the bionic structure in the reference, the bionic structure parameters are defined as follows: The distance from the cutting edge is 80 μm~120 μm, the offset angle is 0.1°~0.5°, the texture has a diameter of 40 μm, the center distance is 80 μm, and the depth is 20 μm; the different textures of the cutting edges are shown in Table 1.

Table 3 Johnson-Cook model parameters of Ti6Al4V

A (MPa)	A (MPa)	n	C	m	T_m (°C)	T_0 (°C)
900	800	0.22	0.014	1.1	1650	25

In order to improve the calculation efficiency, the overall model size is scaled proportionally, and the model size is one fourth of the original model. The diameter of the tool is φ 10 mm, the size of the workpiece is 10 mm × 5 mm × 6 mm, the angle between the surface of the workpiece and the horizontal plane is 15°, the workpiece material is TC4, and the tool material is cemented carbide. The tool-workpiece assembly relationship diagram is shown in Fig. 4. The model was converted to IGES data format and imported into the finite element simulation software Abaqus.

3.2 Cell selection and meshing

In finite element simulation, meshing is the most important step, and the reasonable degree of meshing will directly affect the simulation time and calculation accuracy. In the finite element simulation process, the meshing must be given enough attention. In this study, the blade uses the C3D10M unit, which is a ten-node modified quadratic tetrahedral element. Due to the placement of the texture, the mesh is refined at the cutting edge, and the blade uses a C3D8R unit, which is an

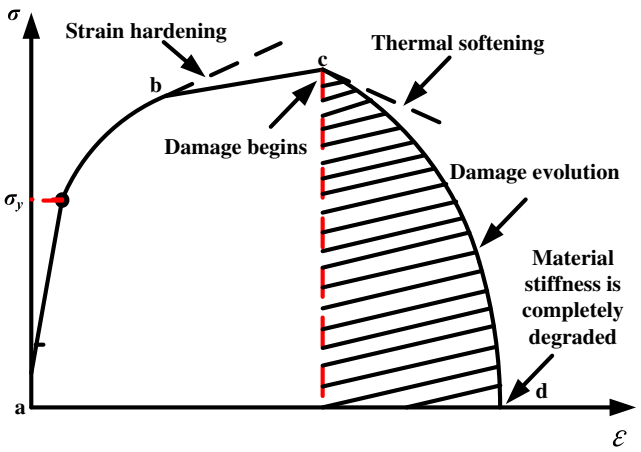

Fig. 6 The stress-strain curve during material failure

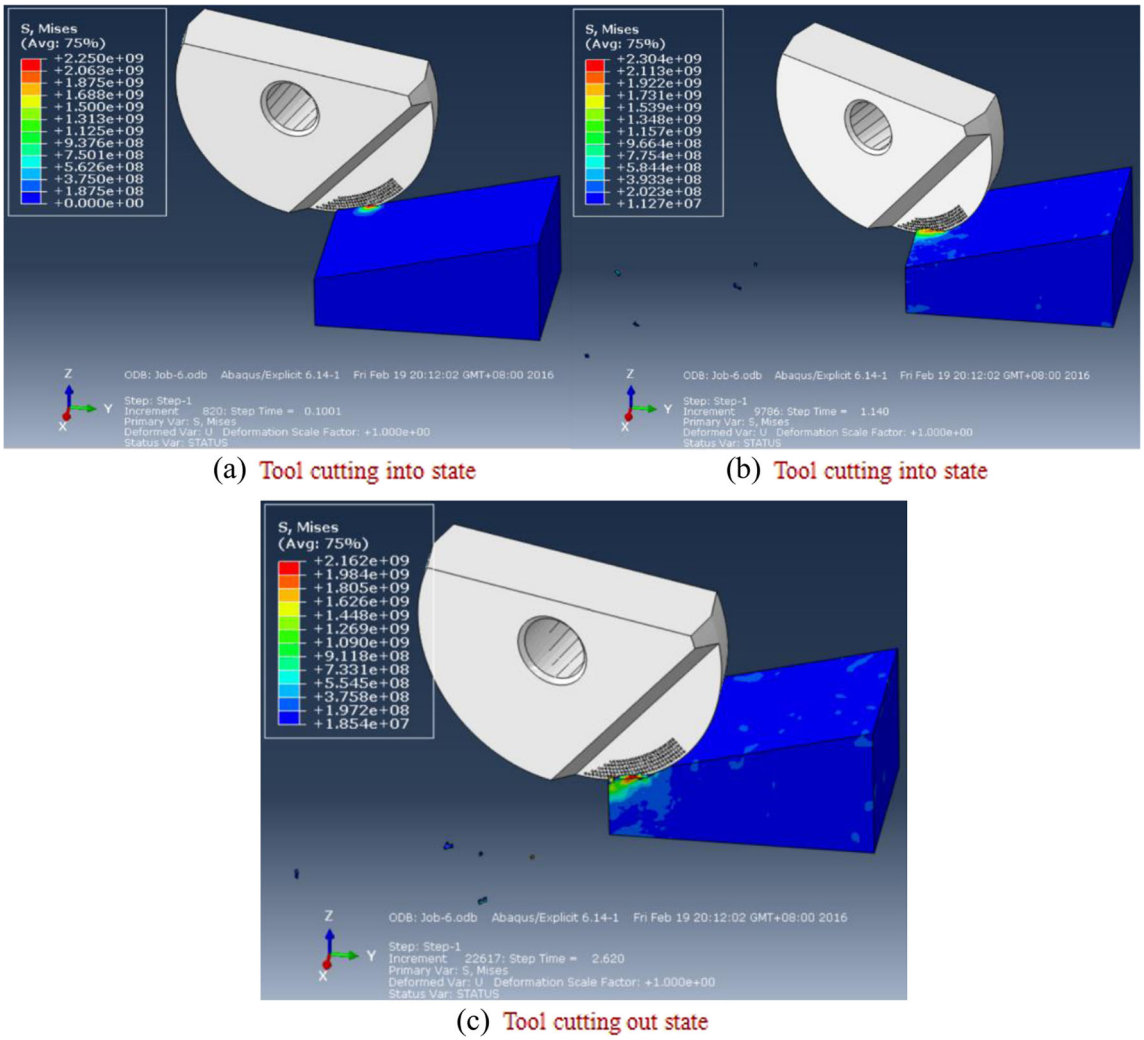

Fig. 7 Finite element simulation process of pit texture cutting

eight-node linear hexahedral unit. Using the unit deletion and second-order accuracy options, the workpiece is judged to be invalid due to the fracture criterion. The finite element model meshing is shown in Fig. 5, and the meshing of the cutting edges of different bionic structure is shown in Table 2.

4 Key technology of finite element simulation process

4.1 Establishment of material model

Whether the numerical simulation results of metal cutting processing can reflect the actual processing depends largely on the establishment of constitutive equations, so it is of great significance to establish accurate material models in finite element simulation. The cutting process has the characteristics of high strain rate, high temperature, and large strain. In many constitutive relation models, the Johnson-Cook model as an ideal rigid-plastic strengthening model can reflect the strain hardening of the material at high strain rate (10^2~10^6 s^{-1}) and can reflect the thermal softening effect. Therefore, selecting the Johnson-Cook model to describe the workpiece material is beneficial to the simulation results closer to the actual situation. The J-C constitutive equation expression is:

$$\overline{\sigma} = \left(A + B\overline{\varepsilon}^{n}\right)\left[1 + C\ln\frac{\dot{\overline{\varepsilon}}}{\dot{\overline{\varepsilon}}_0}\right]\left[1-\left(\frac{T-T_0}{T_m-T_0}\right)^{m}\right] \tag{10}$$

$\overline{\sigma}$ is the equivalent plastic stress, $\overline{\varepsilon}$ is the equivalent plastic strain, $\dot{\overline{\varepsilon}}$ is the equivalent plastic strain rate, $\dot{\overline{\varepsilon}}_0$ is the reference plastic strain rate, T_m is the melting point of the material, and T_0 is usually defined as room temperature 25°. When defined below T_0, material properties are independent of temperature; A, B, C, m, and n are the material initial yield stress, hardening coefficient, strain rate sensitivity coefficient, thermal softening coefficient, and work hardening index, where A, B, C, m, and n are the material constants. The Johnson-Cook model parameters of the Ti6Al4V material are shown in Table 3.

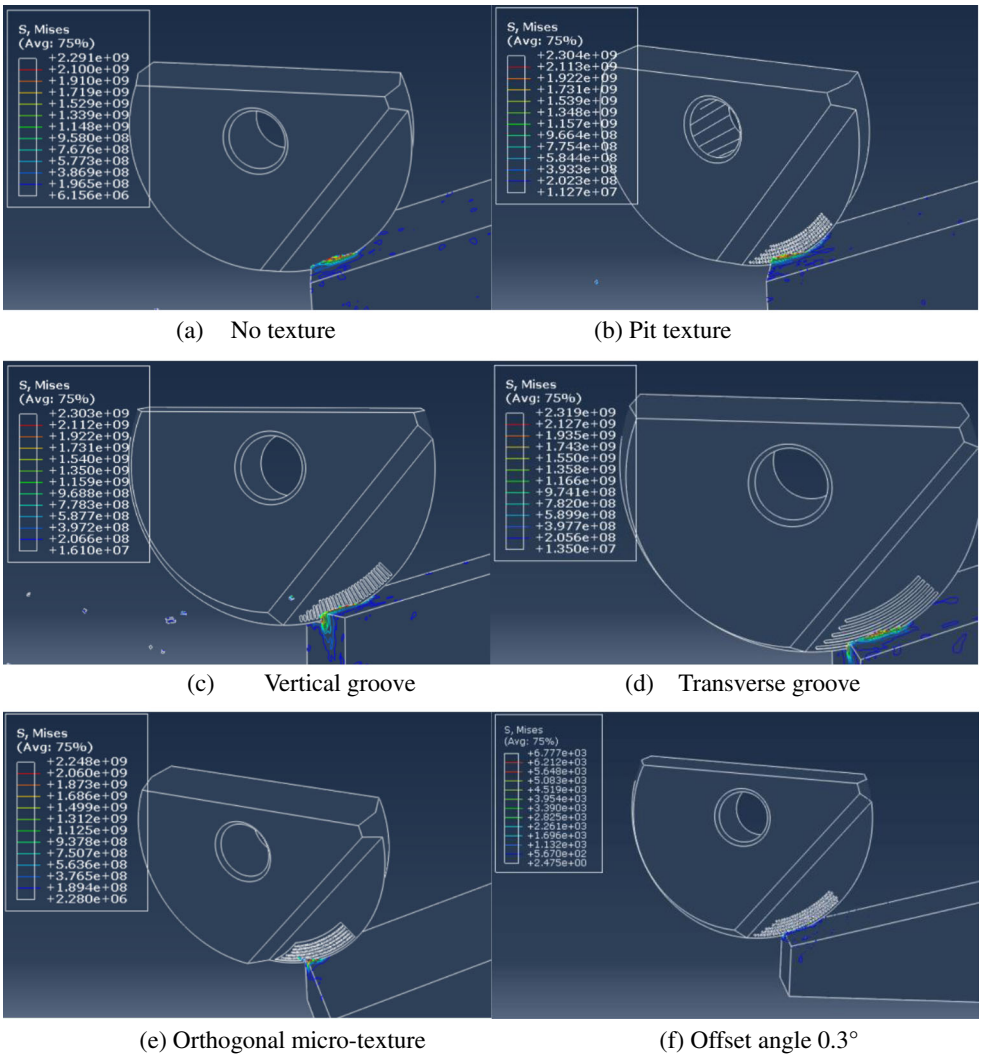

Fig. 8 The stress cloud diagram of the cutting process of different texture types. (**a**) No texture. (**b**) Pit texture. (**c**) Vertical groove. (**d**) Transverse groove. (**e**) Orthogonal micro-texture. (**f**) Offset angle 0.3°

4.2 Establishment of friction model

In the metal cutting process, the friction along the knife-chip interface plays a very important role and must be given a high degree of attention. As the tool cuts into the workpiece and the chip separates from the workpiece, the friction between the tool rake face and the chip is generated. The friction is divided into two regions: One of the areas is from the tip of the knife along the rake face to a certain point, the frictional stress is constant, the area is the viscous friction zone, and the chip is in plastic contact. Another area is the sliding friction zone continuing from the point along the rake face where the knife-chip elastic friction occurs, and the frictional property in this region is that the external friction conforms to the Coulomb friction law. The rules for dividing the viscous friction zone and the sliding friction zone are:

$$\begin{cases} \mu\sigma_{\mathrm{n}} \geq \sigma_{\mathrm{s}} \text{ (Viscous friction zone)} : \tau_{\mathrm{f}} = \sigma_n \\ \mu\sigma_{\mathrm{n}} \geq \sigma_{\mathrm{s}} \text{ (Sliding friction zone)} : \tau_{\mathrm{f}} = \mu\sigma_{\mathrm{n}} \end{cases} \tag{11}$$

τ_{f} is the friction shear stress on the rake face, σ_{s} is the maximum shear stress of the workpiece material, σ_{n} is the normal stress of the rake face, and μ is the coefficient of friction on the rake face.

4.3 Material failure criterion

Whether the sawtooth shape chip can be formed during the high speed cutting of the titanium alloy is related to the parameters used in the fracture criterion, and the selection of the fracture criterion depends entirely on the constitutive model of the selected material. The failure process can be divided into two stages: damage failure of materials and damage evolution of materials. The stress-strain curve during material failure is shown in Fig. 6. Section (a-b) is the stage of elastic deformation of the material. As the stress increases to the yield stress σ_{y}, the material deformation enters the plastic phase from the elastic phase, and the material undergoes strain hardening, section (b-c) is the stage of plastic deformation of the material. As the stress continues to increase to point *c*, the material begins to fail and the equivalent stress of the material begins to

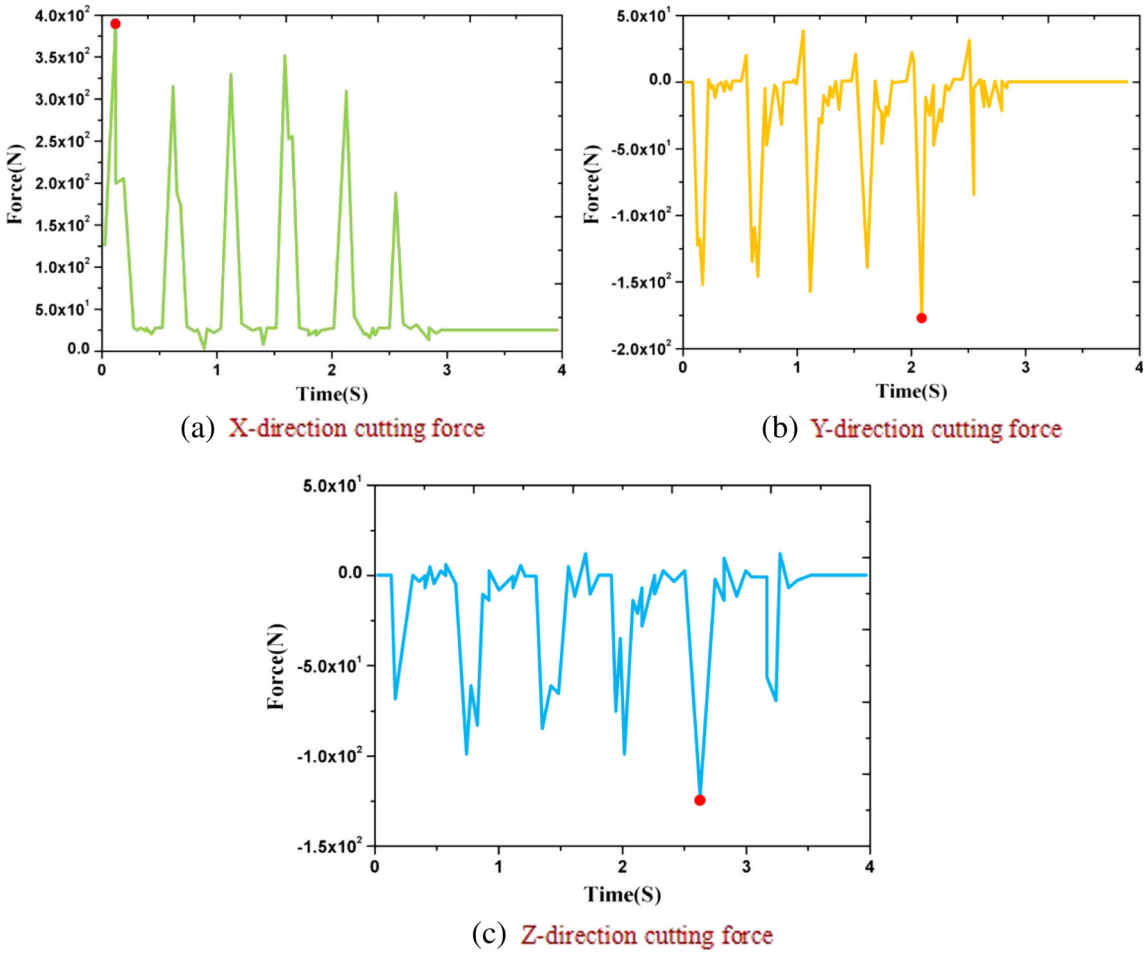

Fig. 9 Non-texturing tool cutting force curve

degrade. Then, the material enters the stage of damage evolution, and the thermal softening phenomenon of the material is very obvious. When the stress reaches the point *d*, the stiffness is completely degraded and the material completely fails.

The expression for the fracture criterion of the Johnson-Cook material model is:

$$\varepsilon_{\mathrm{p}}^{\mathrm{f}} = \left[\mathrm{D1} + \mathrm{D2}\exp\left(\mathrm{D3}\frac{\sigma_{\mathrm{p}}}{\sigma_*}\right)\right] \times \left[1 + \mathrm{D4}\ln\frac{\varepsilon_0}{\varepsilon_{\mathrm{p}}}\right] \times \left[1 + \mathrm{D5}\left(\frac{T-T_0}{T_{\mathrm{m}}-T_0}\right)\right] \quad (12)$$

$\varepsilon_{\mathrm{p}}^{\mathrm{f}}$ is the equivalent plastic strain of failure, σ_{p} is the compressive stress, σ_* is the mean of the three directions of normal stress, ε_{p} is the strain rate, ε_0 is the reference strain rate, and *D*1-*D*2 is the failure parameter of the material.

5 Analysis of cutting simulation results of bionic ball-end milling cutter

5.1 Titanium alloy workpiece surface stress state

Combined with the actual machining situation, the simulated milling parameters are $v_{\mathrm{c}} = 120$ m/min, $f_{\mathrm{z}} = 0.08$ mm/z, $a_{\mathrm{p}} = 0.5$ mm, and $a_{\mathrm{e}} = 0.3$ mm; the finite element simulation process of the pit texture cutting process is shown in Fig. 7. Figure 7a shows the state in which the tool is cut into the workpiece, Fig. 7b shows the state in which the tool is cut, and Fig. 7c shows the state in which the tool is cut out, respectively. Since the ball-end mill cutting process is alternately cutting between the two teeth, the cutting thickness of each tooth is continuously changed. During the cutting process, the tool and the machining surface are closely fitted, and the tool forms a maximum equivalent stress zone at the contact portion of the workpiece, and the shear slip is also the first deformation zone in the region.

The stress cloud diagram of the cutting process of different bionic ball-end mill is shown in Fig. 8. In the undeformed chip distribution, the maximum equivalent stress appears near the cutting edge, and the equivalent stress expands outwardly around the knife-work contact point, the farther away from the cutting area, the smaller the equivalent stress value. There is a significant difference in the maximum equivalent stress value on the surface of the workpiece; the maximum equivalent stress values of the workpiece no texture, pit texture, transverse groove, vertical groove, orthogonal micro-texture, and offset angle of 0.3° are 2468 Mpa, 2301 Mpa, 2322 Mpa, 2368 Mpa, 2386 Mpa, and

2357 Mpa. Compared with the non-textured ball-end mill, the maximum equivalent stress value of the bionic ball-end mill is reduced by 3.5–7.2%, and the equivalent stress area and depth of the non-textured ball-end mill are larger than the bionic ball-end mill. It can be seen that the placement of the biomimetic structure can improve the equivalent stress distribution state of the workpiece surface.

5.2 Analysis of titanium alloy cutting force simulation results

The source of cutting force mainly includes two aspects: On the one hand, during the cutting process of the tool, the surface of the workpiece undergoes elastoplastic deformation to generate resistance. On the other hand is the friction generated between the tool and the chip during the cutting process. Since the friction between the bionic ball-end mill and the chip is reduced, it can be seen that the insertion of the bionic structure can play a role in anti-wear to a certain extent.

The cutting force of the non-texturing tool in the three directions of X, Y, and Z is as shown in Fig. 9. In Fig. 9a, the cutting force in the X direction is 381 N, and the cutting force in the Y direction in Fig. 9b is – 174 N; the cutting force in the Z direction in Fig. 9c is – 126 N. The cutting force of the pit texture tool in the three directions of X, Y, and Z is as shown in Fig. 10. In Fig. 10a, the cutting force in the X direction is 349 N, and the cutting force in the Y direction in Fig. 10b is – 143 N; the cutting force in the Z direction in Fig. 10c is – 124 N. It can be seen from the analysis that the cutting force of the pit texture tool in the X and Y directions is much smaller than that of the non-textured tool, indicating that the placement of the pit texture plays a positive role in reducing the cutting force. Since the ball-end mill does not move in the Z direction, the cutting forces in the Z direction are the same in Figs. 9 and 10.

Figure 11 shows the effect of bionic structure on cutting force. It can be seen from Fig. 11(a) that as the offset angle increases, the cutting force decreases first and then increases. It can be seen from Fig. 11(b) that the cutting force decreases as the distance from the cutting edge increases. It can be seen from Fig. 11(c) that the cutting force of the non-textured tool is large, and the difference in the cutting force between the different bionic structures

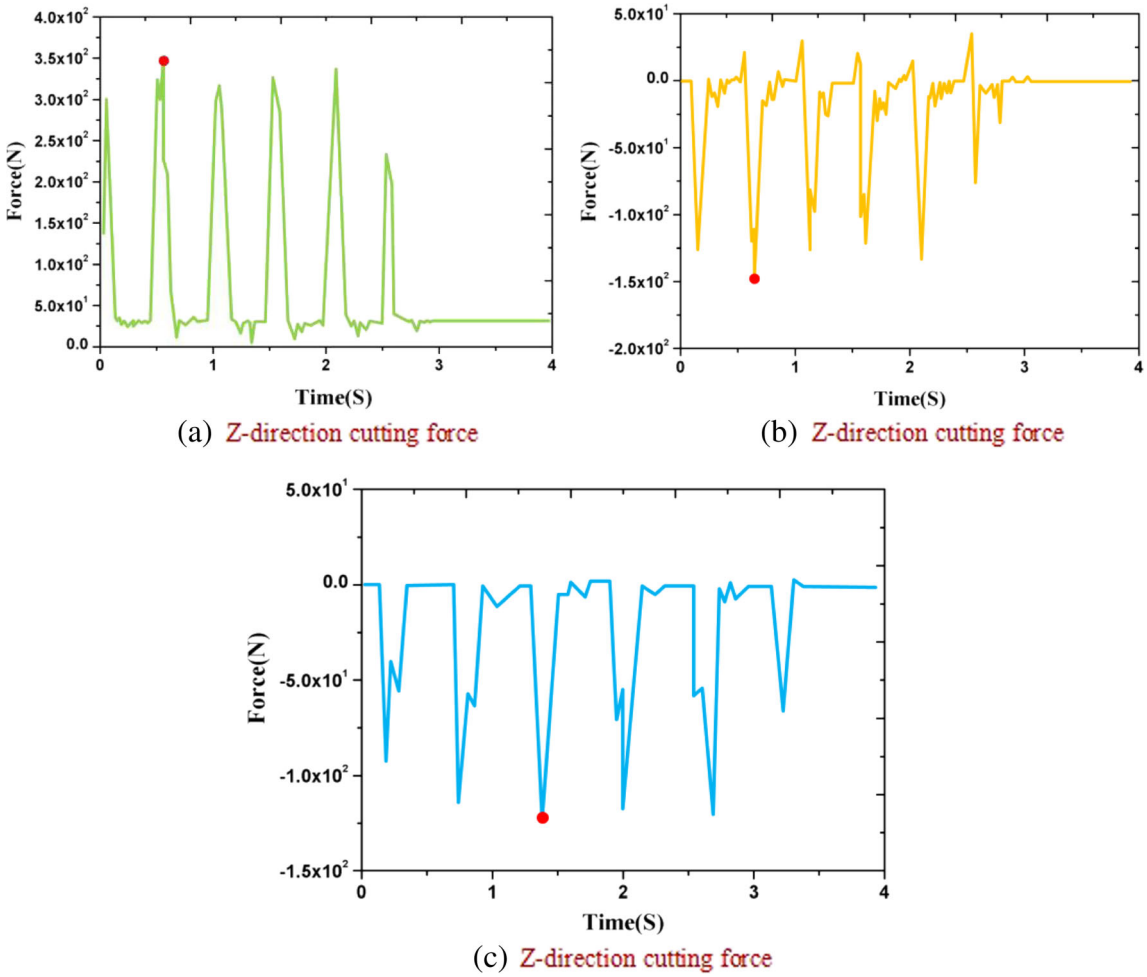

Fig. 10 Pitch texture tool cutting force curve

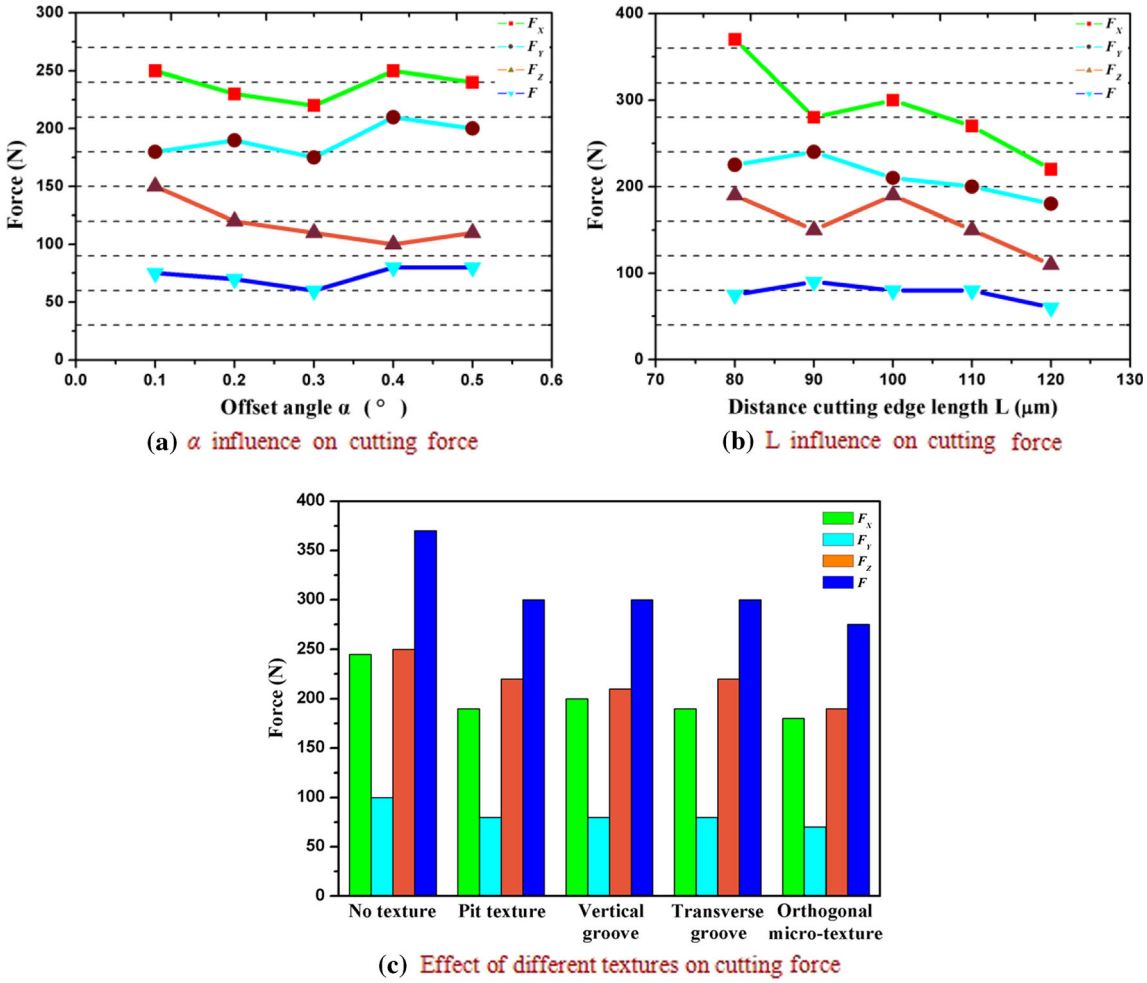

Fig. 11 Effect of bionic structure on cutting force

is not significant. Because of the different arrangement of the bionic structures, the form of the knife-chip contact in the cutting process is different, resulting in different cutting forces. The above results fully demonstrate that the placement of the bionic structure plays a positive role in reducing the cutting force of the tool.

6 Conclusions

According to the processing characteristics of the ball-end milling cutter, the forming process of the machined surface during the cutting process of the ball-end milling cutter is analyzed, and the finite element model of the milling process of the bionic ball-end milling cutter is established to study the cutting force and stress during the processing of bionic ball-end mill; the main research conclusions are as follows:

1. Through the ball-end milling cutter along the bevel cutting geometry, it is concluded that the maximum effective cutting radius of the ball-end milling cutter is reduced when the tool wears, and the cutting speed is reduced, resulting in a change in the cutting environment. Based on the machining characteristics of the ball-end milling cutter, the geometric model of the equivalent cutting thickness is established. It is concluded that the feed per tooth and the tool radius determine the geometry of the chip.
2. The dynamic simulation of the milling bevel process of the bionic ball-end milling cutter is realized. The stress distribution on the surface of the workpiece under different bionic structures is analyzed. It is found that there is a significant difference between the maximum equivalent stress values of the lower workpiece surface of different bionic structures. Bionic ball-end milling cutter and no compared with the maximum equivalent stress value of the textured ball-end milling cutter, the basic equivalent data is reduced by 3.5–7.2%, which provides basic data for the study of the cutting performance of the bionic ball-end mill.
3. The dynamic cutting force curve during the finite element simulation process is obtained, and the influence of bionic

structure, distance from the cutting edge, and offset angle on the cutting force is analyzed. Compared with the non-textured tool, the bionic ball-end milling cutter has stable cutting force and small fluctuation, which fully proves that the placement of the bionic structure plays a positive role in reducing the cutting force of the tool.

Since the continuously changing chips are calculated as the equivalent chips of uniform thickness distribution when calculating the cutting thickness, there is a certain deviation in the calculation process of the cutting thickness. In this paper, the cutting force of the bionic ball-end milling cutter is studied. The cutting temperature is not analyzed. Therefore, the temperature needs to be further discussed.

Funding information This work was supported by the National Natural Science Foundation of China (51775151).

References

1. Etsion I (2005) State of the art in laser surface texturing[J]. J Tribol 127(1):761–762
2. Ryk G, Etsion I (2006) Testing piston rings with partial laser surface texturing for friction reduction[J]. Wear 261(7):792–796
3. Zheng L, Wu J, Zhang S (2016) Bionic coupling of hardness gradient to surface texture for improved anti-wear properties[J]. J Bionic Eng 13(3):406–415
4. Thepsonthi T, Özel T (2013) Experimental and finite element simulation based investigations on micro-milling Ti-6Al-4V titanium alloy: effects of cBN coating on tool wear[J]. J Mater Process Technol 213(4):532–542
5. Kawasegi N, Sugimori H, Morimoto H (2009) Development of cutting tools with microscale and nanoscale textures to improve frictional behavior[J]. Precis Eng 33(3):248–254
6. Zhang K, Deng J, Xing Y (2015) Effect of microscale texture on cutting performance of WC/co-based TiAlN coated tools under different lubrication conditions[J]. Appl Surf Sci 326:107–118
7. Ronen A, Etsion I, Kligerman Y (2001) Friction-reducing surface-texturing in reciprocating automotive components[J]. A S L E Transactions 44(3):359–366
8. Enomoto T, Sugihara T (2010) Improving anti-adhesive properties of cutting tool surfaces by nano−/micro-textures[J]. CIRP Ann Manuf Technol 59(1):597–600
9. Lei S, Devarajan S, Chang Z (2009) A study of micropool lubricated cutting tool in machining of mild steel[J]. J Mater Process Technol 209(3):1612–1620
10. Rao VS, Rao PVM (2005) Modelling of tooth trajectory and process geometry in peripheral milling of curved surfaces[J]. Int J Mach Tool Manu 45(6):617–630
11. Mhamdi MB, Boujelbene M, Bayraktar E (2012) Surface integrity of titanium alloy Ti-6Al-4 V in ball end milling[J]. Phys Procedia 25(22):355–362
12. Senatore J, Segonds S, Rubio W (2012) Correlation between machining direction, cutter geometry and step-over distance in 3-axis milling: application to milling by zones[J]. Comput Aided Des 44(12):1151–1160
13. Jiang Z, Sun J, Xiong Q (2016) Structural design of groove and micro-blade of the end mill in aluminum alloys machining based on bionics[J]. Int J Adv Manuf Technol 88(9–12):1–14
14. Zhong MC (2013) Non-smooth characteristic on biological surface and development of bionics non-smooth diamond bit[J]. Adv Mater Res 712-715(1):360–365
15. Sczerzenie F (2014) The effect of alloy formulation, cold work and inclusion content on micro-void formation in NiTi alloys[J]. Procedia CIRP 13:55–60
16. Yao CF, Dao-Xia WU, Jin QC (2013) Influence of high-speed milling parameter on 3D surface topography and fatigue behavior of TB6 titanium alloy[J]. Trans Nonferrous Metals Soc China 23(3):650–660
17. Honghua SU, Liu P, Yucan FU (2012) Tool life and surface integrity in high-speed milling of titanium alloy TA15 with PCD/PCBN tools[J]. Chin J Aeronaut 25(5):784–790
18. Razfar MR, Zinati RF, Haghshenas M (2011) Optimum surface roughness prediction in face milling by using neural network and harmony search algorithm[J]. Int J Adv Manuf Technol 52(5–8):487–495
19. Ren LQ, Tong J, Li JQ (2001) SW—soil and water: soil adhesion and biomimetics of soil-engaging components: a review[J]. J Agric Eng Res 79(3):239–263
20. Peng F, Wu (2013) Modeling and controlling of surface micro-topography feature in;micro-ball-end milling[J]. Int J Adv Manuf Technol 67(9–12):2657–2670